ELSEVIER

International Journal of Adhesion & Adhesives 29 (2009) 56–66

International Journal of Adhesion & Adhesives

www.elsevier.com/locate/ijadhadh

Experimental and analytical investigations of creep of epoxy adhesive at the concrete–FRP interfaces

Pania Meshgin[a], Kyoung-Kyu Choi[b], Mahmoud M. Reda Taha[c,*]

[a]*Department of Civil Engineering, University of New Mexico, 217 Tapy Hall, MSC01 1070, Albuquerque, NM 87131-0001, USA*
[b]*Department of Architectural Engineering, Dankook University, Yongin-city, Gyeonggi-do 448-701, Republic of Korea*
[c]*Department of Civil Engineering, University of New Mexico, 214 Tapy Hall, MSC01 1070, Albuquerque, NM 87131-0001, USA*

Accepted 10 January 2008
Available online 3 February 2008

Abstract

This paper presents the results of experimental and analytical investigations on the long-term behavior of epoxy at the interface between the concrete and the fiber-reinforced-polymer (FRP). Double shear experiments under sustained service load were performed on nine specimens composed of two concrete blocks connected by FRP sheets bonded to concrete using epoxy. The primary investigation parameters included the ratio of shear stress to ultimate shear strength, the epoxy thickness and the epoxy time-before-loading. Loading was sustained for periods up to nine months. We show that the magnitude of shear stress to ultimate shear strength and the epoxy time-before-loading could be the most critical parameters affecting creep of epoxy at the concrete–FRP interfaces. It was also found that the creep of epoxy can result in failure at the interfaces due to the combined effect of relatively high shear stress to ultimate shear strength and thick epoxy adhesive. This can have an adverse effect on the designed performance of reinforced concrete (RC) structures strengthened with FRP. Based on the experimental observations, rheological models were developed to simulate the long-term behavior of epoxy at the concrete–FRP interfaces. It is shown that the long-term behavior of epoxy at the interfaces can be properly modeled by analytically for both loading and unloading stages.
© 2008 Elsevier Ltd. All rights reserved.

Keywords: Epoxy (A); Concrete (S); Rheology (M); Creep (P)

1. Introduction

As an infrastructure ages, rehabilitation of existing reinforced concrete (RC) structures has emerged as a primary issue to the civil engineering community. In the last decade, the use of fiber-reinforced-polymer (FRP) sheets and plates appeared as a promising alternative to retrofitting materials (i.e. steel) due to advantages of FRP such as high corrosion resistance, durability, and high strength to weight ratio [1,2]. Because of its ease of application, external FRP sheets are recognized as an efficient strengthening alternative for existing RC structures and are being widely used in buildings and bridges [1,2].

However, the performance of RC structures externally strengthened with FRP is highly dependent on the quality of the bond provided by the epoxy adhesive at the concrete–FRP interfaces. Recently, Roberts [3], Ziraba et al. [4], Malek et al. [5] and Ahmed et al. [6] showed that poor quality bonds at the concrete–FRP interfaces result in unexpected stress distribution and significant stress concentration at FRP cut-off points. Such stress concentration can initiate FRP debonding/delamination. Coronado and Lopez [7] found that once the interfacial stresses exceed a threshold value, numerous microcracks develop in the concrete substrate beneath the concrete–epoxy interfaces. Such microcracks can gradually grow to macrocracks and cause premature failure at the interface. Moreover, Teng et al. [8] and Hiroyuki and Wu [9] recognized that shear strength does not increase with increases in the concrete–FRP bond length beyond a minimum length that has been

*Corresponding author. Tel.: +1 505 277 1258.
E-mail address: mrtaha@unm.edu (M.M. Reda Taha).

0143-7496/$ - see front matter © 2008 Elsevier Ltd. All rights reserved.
doi:10.1016/j.ijadhadh.2008.01.003

recognized as necessary to achieve the required shear strength [10].

While the shear–slip relationship at the concrete–FRP interfaces and the delamination mechanism have been examined by many researchers [5,6,10–12], all these studies focused on delamination mechanisms for applied stress close to the ultimate shear strength of the interface. There is a paucity of knowledge about the long-term behavior of the concrete–FRP interfaces subjected to sustained service loads that cause linear elastic deformation at the interface for stress levels much lower than the ultimate shear strength of the interface. Moreover, the fact that such interfaces incorporate three different materials (concrete, epoxy adhesive and FRP) makes complex long-term behavior where creep plays an important role a possibility.

In this article, we present our experimental investigations, using a double shear test set-up, that were performed to examine the long-term behavior of epoxy adhesive at the concrete–FRP interfaces. Three primary parameters were considered: the ratio of sustained shear stress to ultimate shear strength, the time-before-loading and the thickness of the epoxy adhesive layer. Based on experimental observations, several rheological models were developed and examined to simulate the long-term behavior of epoxy at the concrete–FRP interfaces. Researchers showed that analysis of the time-dependent stress of FRP-strengthened RC structures is necessary for realistic prediction of cracking probability [13,14]. Such analysis of time-dependent stress, by means of the finite element method, requires the availability of time-dependent constitutive relations of the interface materials: concrete, FRP and the epoxy adhesive [13]. There is a need for efficient models that can describe the time-dependent behavior of epoxy adhesive at the concrete–FRP interfaces accurately for realistic realization of time-dependent behavior of the interfaces. The effect of temperature on creep of the epoxy adhesive is not considered here because of the limited change in temperature in concrete structures under service conditions. Further research is underway to examine that effect.

2. Experimental methods

Experimental investigation on creep of epoxy at concrete–FRP interfaces was performed by means of a double shear test method as described below.

2.1. Materials

A specific concrete was used to avoid premature failure at the concrete side of the test specimen during the experiment. The concrete mix consists of 1750 kg/m^3 sand; 500 kg/m^3 Type I Portland cement; 282 kg/m^3 water; and superplasticizer. In each concrete batch, three $50 \times 50 \times$ 50-mm cubes for the compressive test and three $50 \times 50 \times$ 110-mm double shear test specimens were cast. All concrete specimens were cured in a water bath at a fixed temperature of 20 °C for seven days. Compressive tests after 28 days were performed according to ASTM standards [15] on six cubes, and a mean compressive strength of 38 MPa ($\pm$3.7 MPa) was achieved for the concrete.

Table 1
Material ingredient of the epoxy adhesive

Ingredient of resin (%)	Epichlorohydrin: 60–100 Silica: 1–5
Ingredient of hardener (%)	Polymercaptan: 60–100 Phenol: 5–10 Silica: 5–10 Ethylene glycol: 1–5
Specific gravity	1.16
Shear strength after 1 h curing (MPa)	10.3
Shear strength after 24 h curing (MPa)	13.7

Carbon fiber reinforced polymer (CFRP) sheets were used in this research. CFRP sheets were made of PANEX@35 carbon fiber, formed from high capacity PAN processing methods. Based on the manufacturer's data sheets, the tensile strength and tensile modulus of elasticity of the carbon fiber sheets, which do not include saturant, were 3860 MPa and 242 GPa, respectively.

A fast setting, low odor epoxy adhesive, made of epichlorohydrin resin and polymercaptan hardener was used as an adhesive. Mixing two different components (the resin and the hardener) forms the adhesive. Material properties of the epoxy are presented in Table 1. The ultimate shear strength at the concrete–FRP interfaces was tested on six double shear specimens made of the above concrete, epoxy, and CFRP materials. The mean ultimate shear strength was found to be 0.56 MPa ($\pm$0.107 MPa). Failure of double shear specimens occurred by delamination of the concrete layer directly bonded to FRP.

2.2. Creep test set-up

The double shear test specimen consisted of two $50 \times 50 \times 110$-mm concrete blocks connected by two $0.39 \times 35 \times 150$-mm FRP sheets with epoxy adhesive (Fig. 1). Each concrete block was cured for 3–7 days in air after being cured for 28 days in a water bath to allow concrete shrinkage to develop. Fig. 2(a) shows the test setup used in the shear creep test. The concrete block was attached to a horizontal steel cantilever frame supported on a roller at one end and fixed to the table at the other end. As shown, the load was applied to the specimen by means of a sustained dead weight applied at the other end of the cantilever. The use of a cantilever test setup is a well-established technique for generating sustained creep loads [16]. Each specimen had an 8-mm diameter steel bar going through a polymer sleeve 13 mm in diameter to prevent friction between the concrete and the steel bar (Fig. 1). The steel bar was connected to a steel plate, $50 \times 50 \times 6$ mm, to uniformly distribute the applied compressive force to the concrete block.

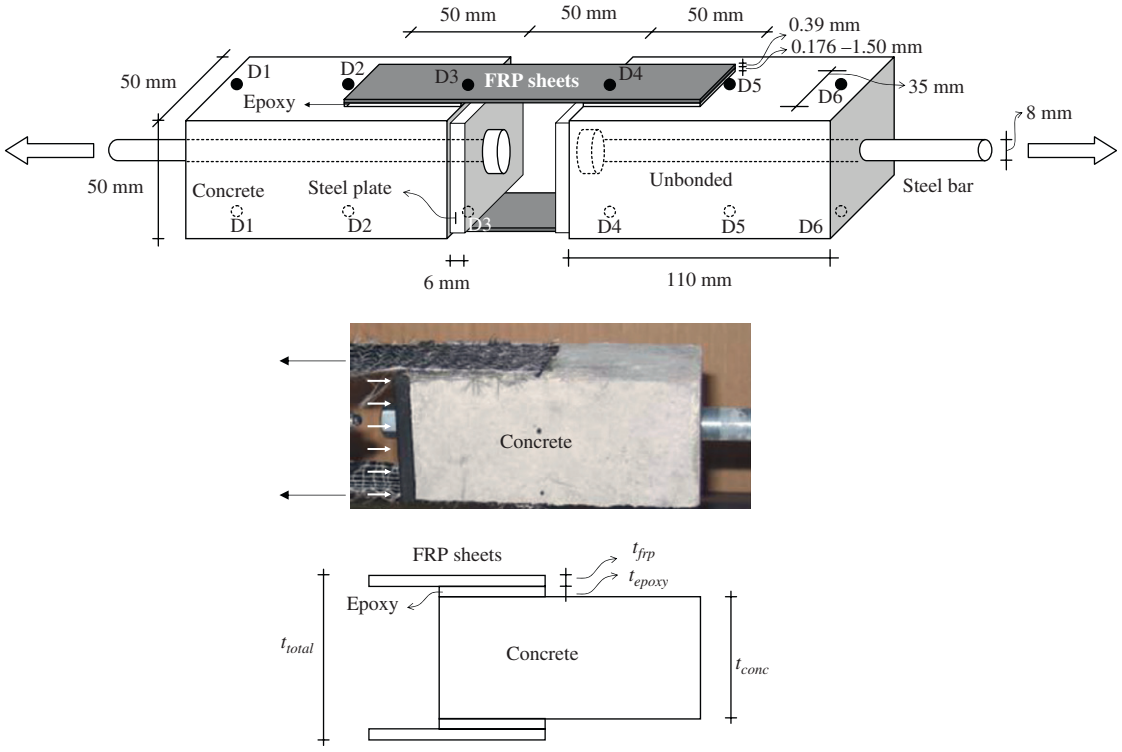

Fig. 1. Creep test specimen.

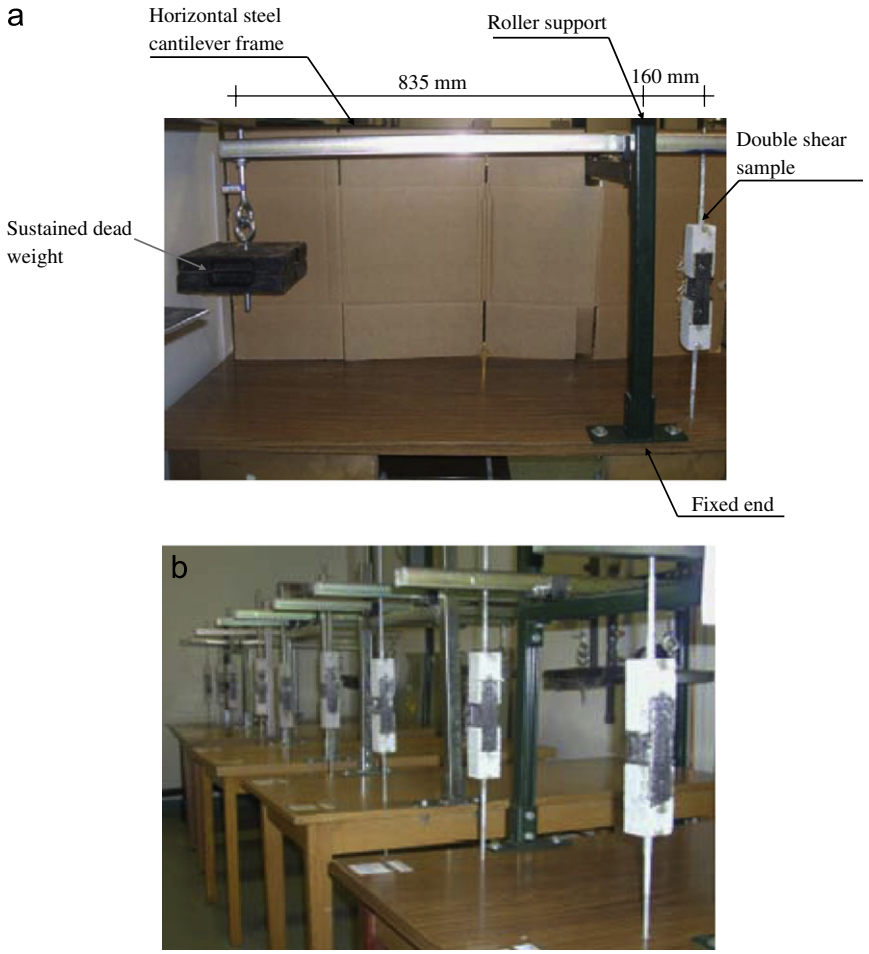

Fig. 2. Shear creep test set-up.

Table 2
Properties of test specimens

Specimens	τ/τ_{ult}	Time-before-loading (Day)	t_{epoxy} (mm)
S1-F	0.22	1	0.21
S1-B	0.18	1	0.21
S2-F	0.30	1	0.18
S2-B	0.33	1	0.18
S3-F	0.15	1	0.24
S3-B	0.15	1	0.24
S4-F	0.61	1	0.28
S4-B	0.64	1	0.28
S5-F	0.21	7	0.21
S5-B	0.11	7	0.21
S6-F	0.35	7	0.21
S6-B	0.27	7	0.21
S7-F	0.47	7	0.17
S7-B	0.77	7	0.17
S8-F	0.28	1	1.50
S8-B	0.34	1	1.50
S9-F	0.47	1	1.65
S9-B	0.78	1	1.65

In the present study, three variables were examined: ratio of shear stress to ultimate shear strength, epoxy thickness, and time-before-loading, which is defined as the time period between the time of application of epoxy and the loading time and is denoted as t_c. Nine specimens were tested under laboratory conditions controlled to constant temperature (23 ± 2 °C), while the relative humidity (RH) ranged between 40% and 55%. Properties of the test specimens are presented in Table 2. The nine test frames are shown in Fig. 2(b). These nine specimens included four different nominal shear stresses to the ultimate shear strength ratio of 15%, 20%, 31% and 62%, two different time-before-loading values of one day and seven days, and eight different thicknesses of epoxy adhesive. It should be noted that the applied shear stress at front and back faces of the specimens were not necessarily equal due to small differences in interface characteristics at both faces. These differences between the two sides of the specimens are mainly attributed to difference in surface roughness of concrete, which existed even when a specific roughness was targeted before applying epoxy. Based on theory of elasticity, the shear stress applied at each face was evaluated by considering the measured instantaneous deformation (Table 2). Details of the calculation of the stress based on measured deformation are described in Appendix A. It is noted that the maximum shear stress did not exceed 80% of the ultimate shear strength thereby simulating a realistic service load similar to those observed in RC structures strengthened with FRP sheets.

According to the manufacturer's data sheets for epoxy, 90% of the mechanical capacity of epoxy would be achieved after 24 h of cure and the full material strength would be achieved after 3 days of cure. The choice of one and seven days for time-before-loading was to investigate the effect of the extreme limits of time-before-loading on creep at the concrete–FRP interfaces. The different epoxy thicknesses were achieved by adding extra layers of epoxy prior to applying FRP. It should be noted that each extra layer of epoxy was applied 20 min after the application of the previous layer to allow the previous layer to dry. Eq. (1) was used to determine the average epoxy thickness for each specimen (see Fig. 1).

$$t_{epoxy} = \frac{t_{total} - t_{conc} - 2t_{frp}}{2}, \quad (1)$$

where t_{total} is the total thickness of the concrete–FRP interface, t_{conc} the thickness of the concrete block and t_{frp} the thickness of the FRP sheet which is 0.39 mm. The values of t_{total} and t_{conc} were the mean values of 40 measurements, and t_{frp} is based on the FRP manufacturer data sheet. All the thicknesses were measured with a digital micrometer having 0.001 mm resolution. Accurate measurement showed that the front and back faces had almost equal epoxy adhesive thicknesses. Therefore, a mean thickness can be used as in Eq. (1). Table 2 presents the properties of each specimen with front and back faces denoted F and B.

The shear deformation was measured by observing the displacement of six gauge points (DEMEC® gauge points) fixed at front and back faces on the specimens. Fig. 1 shows the location of these gauge points denoted as D1–D6. By considering the change in distance between these gauge points, the creep displacement was computed as discussed below. The distance between these fixed gauge points was measured with 0.001 mm resolution. The distances between D1 and D3 and between D5 and D6 were also measured to compensate for concrete shrinkage. The experimental observations showed that concrete shrinkage strains were insignificant compared with the creep strains of epoxy. The insignificant shrinkage was due to the fact that the concrete specimens were left in the dry laboratory environment at (40–55%) RH for 3–7 days before load application.

It should be noted that in field applications of FRP sheets to concrete, a wet lay-up process is usually used [18]. In this process, two types of resins, known as saturant resin and adhesive resin, are used [18]. However, the saturant resin was not used in this research so that the complexity associated with creep of the saturant resin could be avoided. By excluding the saturant resin, and knowing the fact that creep of the carbon fiber sheets is insignificant [19,20], we were able to use the above test setup and experiments to study creep of the epoxy adhesive at the concrete–FRP interfaces.

2.3. Load history

In this paper, long-term behavior of epoxy adhesive at the concrete–FRP interfaces was examined for both loading and unloading. Since the loading frame is statically determinate and the applied weight was sustained, problems associated with hydraulic pressure used for loading, such as the need for reloading, were not encountered here

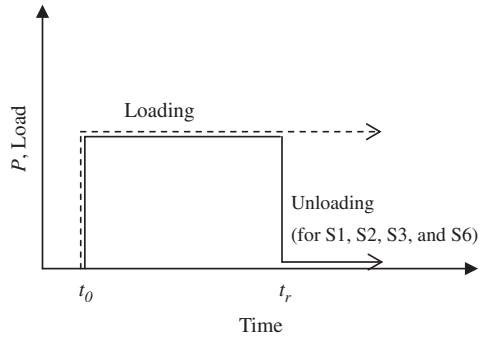

Fig. 3. Load history.

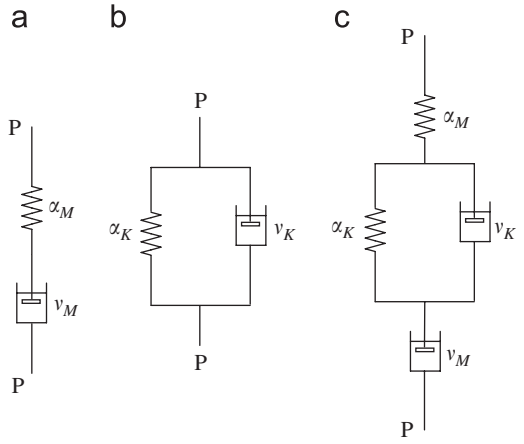

Fig. 4. Existing rheological models. (a) Maxwell model, (b) Kelvin model and (c) Burgers model.

[16,17]. Fig. 3 shows the load history according to time. After time t_0, the specimens were subjected to the sustained load for up to nine months. Specimens S1, S2, S3 and S6 were unloaded at time t_r to investigate creep recovery due to unloading.

3. Rheological modeling

Rheological models have been promoted as effective tools for simulating linear and nonlinear viscoelastic behavior [21]. Many researchers have encouraged the use of these models, because they can provide physical understanding of instantaneous and time-dependent behavior. Rheological models consist of combinations of springs (Hookean element), dashpots (Newtonian liquid) and/or friction elements to simulate the non-linear time-dependent behavior of materials. These models range from classical models like Maxwell and Kelvin models to complex models consisting of numerous springs and dashpots [21]. The classical models (Maxwell and Kelvin models) are composed of one spring and one dashpot as shown in Fig. 4 (a) and (b) described by Eqs. (2) and (3), respectively,

$$x = \frac{Pt}{v_{\mathrm{M}}} + x_{\mathrm{e}}, \tag{2}$$

where x is the total deformation at time t, P the sustained load, x_{e} the instantaneous deformation, and v_{M} the viscosity of the dashpot fluid.

$$x = P\alpha_{\mathrm{K}}(1 - \mathrm{e}^{-t/t_1}), \tag{3}$$

where α_{K} is the spring compliance, $t_1(=\alpha_{\mathrm{K}} v_{\mathrm{K}})$ the retardation time.

These two classical models provide simple mathematical descriptions for the load–deformation relationships that describe the long-term behavior of viscoelastic materials subjected to sustained stress. Rheological models have been developed to simulate the time-dependent behavior in construction materials like concrete [22], masonry [17,23] and wood plastic composites [24]. The Maxwell model overestimates the long-term deformation because of its use of linear relation with time, and the Kelvin model does not consider the instantaneous deformation. Due to the limited ability of these simple models in simulating creep behavior of epoxy adhesives, complex models such as those by Burgers, Findley, Ross, Flugge, Hanse, Cowan and Freudenthal were developed for better simulation of long-term deformation [16,21].

Here, we focus on Burgers (Fig. 4(c)) and Findley models as example rheological models [16] that can provide good simulation with a limited number of modeling parameters. Burgers model consisting of two springs and two dashpots and its load (P)-deformation (x) relationship can be described as

$$x = P\alpha_{\mathrm{M}} + \frac{Pt}{v_{\mathrm{M}}} + P\alpha_{\mathrm{K}}(1 - \mathrm{e}^{-t/t_{\mathrm{K}}}), \tag{4}$$

where α_{M} is the spring compliance of Maxwell branch, v_{M} the viscosity of the dashpot fluid in Maxwell branch, α_{K} the spring compliance of Kelvin branch, $t_{\mathrm{K}}(=\alpha_{\mathrm{K}} v_{\mathrm{K}})$ the retardation time, and v_{K} the viscosity of the dashpot fluid of Kelvin branch. On the other hand, Findley model is a simple power-law model based on a linear viscoelastic approach, which can be described as [25]

$$\varepsilon = \varepsilon_{\mathrm{e}} + (mt^n), \tag{5}$$

where ε is the total strain at time t, ε_{e} the instantaneous strain, and m and n the analytical coefficients which can be defined based on the experimental results.

Furthermore, we suggest a modification to the Maxwell model. We name the new proposed model the modified Maxwell (MM) model. Fig. 5 shows the MM model consisting of two springs and a dashpot. Since the total deformation is equal to the deformation in each branch shown in Fig. 5, the deformation in branch I can be defined as

$$\frac{\mathrm{d}x}{\mathrm{d}t} = \frac{P_1}{v} + \alpha_1 \frac{\mathrm{d}P_1}{\mathrm{d}t}, \tag{6}$$

where x the time dependent deformation at time t, P_1 the load applied to branch I, α_1 the spring compliance of branch I, and v the viscosity of the dashpot fluid in branch I. Similarly, the rate of change of deformation with time in

branch II can be

$$\frac{dx}{dt} = \alpha_2 \frac{dP_2}{dt}, \tag{7}$$

where P_2 is the load applied to branch II and α_2 the spring compliance of branch II. Since the summation of the load $(P_1 + P_2)$ in the two branches is equal to the applied sustained load (P), the variation of total applied load, $dP/dt[= (dP_1/dt + dP_2/dt)]$ is equal to zero. Therefore, by considering force equilibrium the following equation can be obtained as

$$\frac{dx}{dt} = \frac{\alpha_2 P - x}{v(\alpha_1 + \alpha_2)}. \tag{8}$$

Integrating Eq. (8), the load displacement equation can be described as

$$x = P\alpha_2 - (P\alpha_2 - x_e)e^{-t/(v(\alpha_1+\alpha_2))}, \tag{9}$$

where x is the total deformation of epoxy excluding FRP deformation at time t that is equal to $\Delta_{16}(t) - \Delta_{16,FRP}(t)$ shown in Fig. 6, and x_e the instantaneous deformation of epoxy that is equal to $\Delta_{16}(t_0) - \Delta_{16,FRP}(t_0)$. $\Delta_{16}(t)$ and $\Delta_{16}(t_0)$ indicate the total deformation (instantaneous plus creep) at the time t and the instantaneous deformation at the time t_0 between the gauge points D1 and D6 after compensation for concrete shrinkage, and $\Delta_{16,FRP}(t)$ and $\Delta_{16,FRP}(t_0)$ indicate the FRP deformation (instantaneous plus creep) at the time t and the instantaneous deformation at the time t_0 (time of load application), respectively. Considering the fact that carbon fiber develops very negligible creep deformation [18] it is assumed that $\Delta_{16,FRP}(t)$ at time t is equal to the instantaneous FRP deformation $\Delta_{16,FRP}(t_0)$. It should be noted that, since the applied shear stress level at the FRP–concrete interfaces is significantly lower than the shear plastic limit (only 4% of the shear strength of epoxy), only viscoelasticity and not viscoplasticity [26] was considered in the present study.

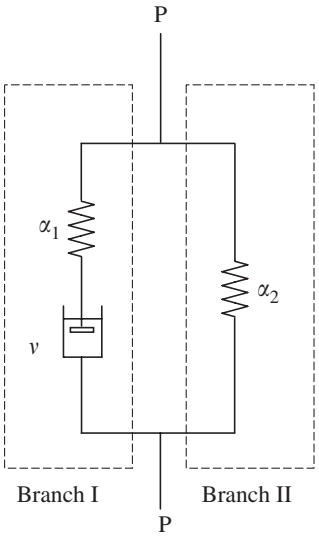

Fig. 5. Proposed rheological model.

4. Results and discussion

Fig. 7 shows example creep results of creep of epoxy adhesive at the concrete–FRP interfaces. The creep coefficient is defined as γ_{cr}/γ_e, where γ_{cr} and γ_e are shear creep strain and instantaneous shear strain of epoxy, respectively. In Fig. 7(a), the specimens, S3-F and S5-B, have two different times-before-loading $t_c = 1$ day and $t_c = 7$ days, respectively. All other parameters in S3-F and S5-B including the magnitude of shear stress and the epoxy thickness were similar. It can be observed that while the two specimens have different creep rates, S3-F with a short time-before-loading ($t_c = 1$ day) shows more ultimate creep deformation than S5-B with a long time-before-loading ($t_c = 7$ days). Therefore, it is evident that as time-before-loading decreases, ultimate creep deformation increases. In Fig. 7(b), creep in specimen S2-F, which has relatively high shear stress to ultimate shear strength ($\tau/\tau_{ult} \approx 0.30$), is compared with creep in specimen S3-F, which has low shear stress to ultimate shear strength ($\tau/\tau_{ult} \approx 0.15$). It can be observed that as the sustained shear stress increases, more ultimate creep develops. These findings were observed in all test specimens. The time axis in Fig. 7 is presented on a logarithmic scale to show the significant amount of creep strain occurring at relatively early times when the stress-to-ultimate-strength ratio is increased.

Fig. 8 shows the time dependent behavior of specimens S9-B, with relatively thick epoxy layer ($t_{epoxy} = 1.65$ mm), subjected to high shear stress levels ($\tau/\tau_{ult} = 0.78$) and a short time-before-loading (1 day). It is noted that specimen S9-B failed 65 days after loading due to debonding of epoxy at the interfaces. Creep strain increased in a nonlinear fashion (primary creep), then it continued to

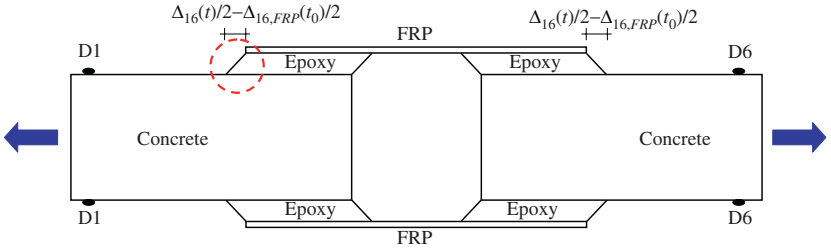

Fig. 6. Shear creep deformation at concrete–FRP interfaces.

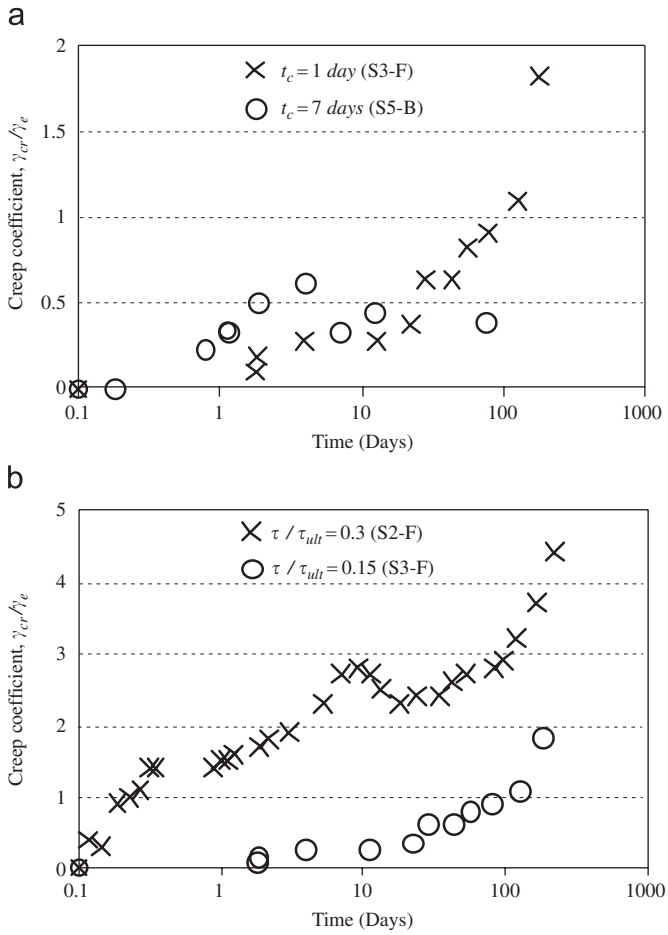

Fig. 7. Example results of creep coefficient of epoxy at the concrete FRP interfaces: (a) effect of time-before-loading and (b) effect of shear stress to shear strength.

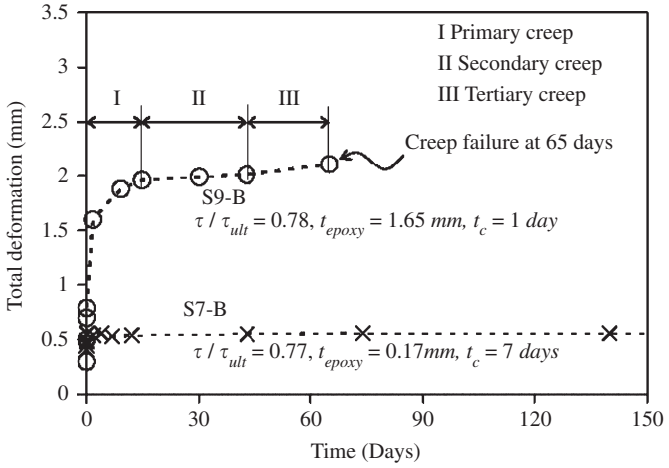

Fig. 8. Time dependent behavior of specimen (S7-B) and specimen (S9-B) showing creep failure. Both specimens have high shear stress to ultimate shear strength.

Table 3
Modeling parameters of Findley model in loading stage

Specimen	Time-before-loading (Day)	*m*	*n*
S1-F	1	0.194	0.210
S1-B	1	0.095	0.359
S2-F	1	0.222	0.183
S2-B	1	0.231	0.191
S3-F	1	0.068	0.250
S3-B	1	0.058	0.200
S4-F	1	0.156	0.024
S4-B	1	0.110	0.012
S5-F	7	0.141	0.191
S5-B	7	0.156	0.121
S6-F	7	0.153	0.165
S6-B	7	0.127	0.165
S7-B	7	0.225	0.116
S8-B	1	0.076	0.130
S9-B	1	0.135	0.204

increase linearly at a much lower rate (secondary creep). Finally, creep strain increased significantly until the specimen failed. Such creep behavior at the final stage is well known as tertiary creep [16,21]. These three stages are shown in Fig. 8. It is important to note that such behavior was only observed for the specimen with a high ratio of shear stress to ultimate shear strength. While it is difficult to draw general conclusions from our limited number of experiments, it is evident that further research is needed to examine the significance of high shear stress to ultimate shear strength combined with a thick epoxy adhesive layer on creep behavior of epoxy at the concrete–FRP interface. We also anticipate that dealing with average values of large number of specimens (once it becomes available) might enable reducing the scatter in the experimental observations reported here.

In the present study, based on the experimental observations, modeling parameters describing rheological models were evaluated by applying principles of system identification for curve fitting. This process identifies the values of the rheological model parameters necessary to minimize the root mean square error between the prediction of the rheological models and the experimental data observed from the creep experiments. Moreover, predictive equations for those modeling parameters were proposed. In this study, the experimental data were divided into a training group for developing the predictive equations of rheological models and a testing group for validating these models.

Numerical analysis for system identification showed both Kelvin and Burgers models to have severe convergence problems. This might be attributed to the limited ability of both models to describe nonlinear viscoelasticity, a limitation observed by other researchers [17]. Therefore, the predictive equations for these models were not further developed here.

The model parameters of the Findley model in the loading stage are presented in Table 3. According to the experimental results, the creep behavior showed significant differences according to time-before-loading. Therefore,

Table 4
Modeling parameters of Burgers model in loading stage

Specimen	Time-before-loading (day)	α_M (mm/N)	α_k (mm/N)	v_M (N day/mm)	v_k (N day/mm)
S1-F	1	0.015	8.89E−5	6.94E−4	6.94E−4
S1-B	1	0.015	8.93E−5	6.94E−4	6.94E−4
S2-F	1	0.0004	−4.74E6	6.49E5	7.02E5
S2-B	1	0.0004	−1.95E6	6.01E5	6.01E5
S3-F	1	−0.0052	−1.20E10	0.0164	9.92E4
S3-B	1	−0.0051	−4.97E9	0.0164	9.91E4
S4-F	1	−0.0037	−2.31E9	0.00564	1.29E6
S4-B	1	−0.0037	−7.33E7	0.00562	1.28E6
S5-F	7	_[a]	_[a]	_[a]	_[a]
S5-B	7	_[a]	_[a]	_[a]	_[a]
S6-F	7	_[a]	_[a]	_[a]	_[a]
S6-B	7	_[a]	_[a]	_[a]	_[a]
S7-B	7	_[a]	_[a]	_[a]	_[a]
S8-B	1	−1.65	−2.76E10	0.00412	3.21E8
S9-B	1	−1.01	−1.12E10	0.00412	1.52E8

[a]Experimental data sets where Burgers model did not converge resulting in negative modeling parameters.

the predictive equations for modeling parameters (m and n) are defined as functions of the ratio of the shear stress to the ultimate shear strength (τ/τ_{ult}), based on Table 3.

For $t_c = 1$ day

$$m = 0.075\left(\frac{\tau}{\tau_{ult}}\right) + 0.10, \tag{10a}$$

$$n = -0.51\left(\frac{\tau}{\tau_{ult}}\right) + 0.37 \geqslant 0. \tag{10b}$$

For $t_c = 7$ days

$$m = 0.13\left(\frac{\tau}{\tau_{ult}}\right) + 0.12, \tag{11a}$$

$$n = -0.15\left(\frac{\tau}{\tau_{ult}}\right) + 0.23 \geqslant 0. \tag{11b}$$

It should be noted that the parameters, m and n, were calculated with minutes as a time unit. Likewise, the modeling parameters of Burgers and the proposed MM models in the loading stage are presented in Tables 4 and 5. Experimental data sets S1-F, S1-B, S2-F, S2-B, S3-F, S3-B, S4-F, S4-B, S5-F, S5-B, S6-F, S6-B, S7-B, S8-B, and S9-B were used in developing both models while experimental data sets S7-F, S8-F, and S9-F were used in the verification of both models. In Table 4, it can be observed that Burgers model showed convergence problems with some experimental data sets. One serious problem was negative values for Burgers model parameters, which negated the physical definition of these parameters. Therefore, Burgers model was not considered any further in the discussion below. Fig. 9 shows the variation of modeling parameters (α_1, α_2 and τ) of MM model according to the magnitude of shear stress to ultimate shear strength (τ/τ_{ult}). In Fig. 9, for one day time-before-loading ($t_c = 1$ day), as τ/τ_{ult} increases, the modeling parameters (α_1, α_2, and τ) decrease until they reach a minimum. For seven days time-before-loading ($t_c = 7$ days), the modeling parameters do not show significant variations according to τ/τ_{ult}. Values of modeling parameters for seven days time-before-loading are almost equal to the minimum for one day time-before-loading ($t_c = 1$ day). Based on this finding, shown in Fig. 9, prediction equations for α_1, α_2, and τ were developed as functions of the shear stress to the ultimate shear strength ratio (τ/τ_{ult}).

Table 5
Modeling parameters of MM model in loading stage

Specimen	Time-before-loading (day)	α_1 (mm/N)	α_2 (mm/N)	v (N day/mm)
S1-F	1	68.8	0.0037	0.025
S1-B	1	179	0.0045	0.062
S2-F	1	19.0	0.0012	0.056
S2-B	1	15.1	0.0013	0.115
S3-F	1	364	0.0015	0.115
S3-B	1	221	0.0014	0.012
S4-F	1	2.40	0.0004	0.001
S4-B	1	2.20	0.0005	0.001
S5-F	7	15.4	0.0018	0.023
S5-B	7	6.40	0.0012	0.008
S6-F	7	12.2	0.0008	0.012
S6-B	7	15.8	0.0007	0.010
S7-B	7	10.5	0.0009	0.005
S8-B	1	13.8	0.0015	0.007
S9-B	1	16.8	0.0011	0.009

For $t_c = 1$ day

$$\alpha_1 = 500 - 2000\left(\frac{\tau}{\tau_{ult}}\right) \geqslant 10 \text{ mm/N}, \tag{12a}$$

$$\alpha_2 = 0.006 - 0.014\left(\frac{\tau}{\tau_{ult}}\right) \geqslant 0.0008 \text{ mm/N}, \tag{12b}$$

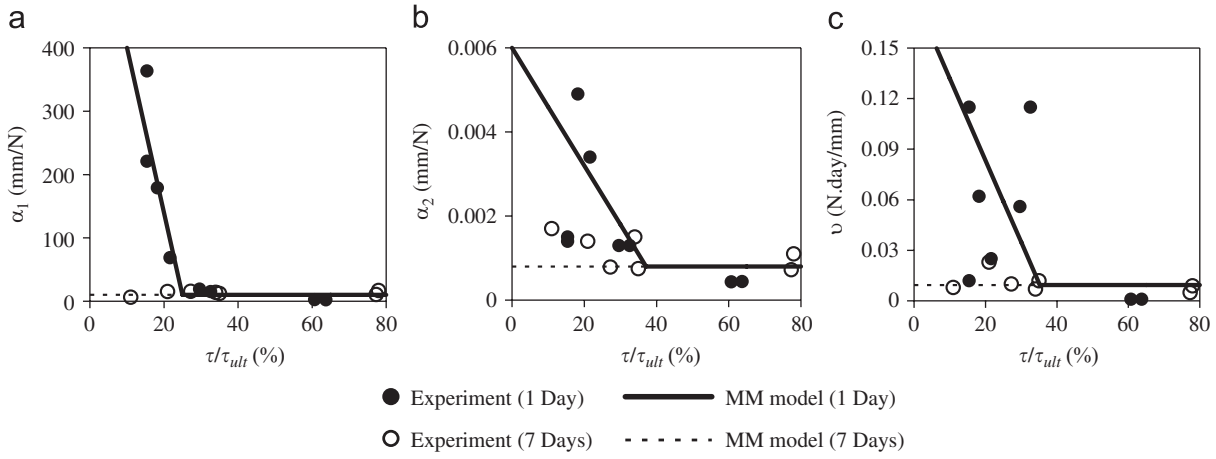

Fig. 9. Variation of modeling parameters of MM model according to time-before-loading and shear stress.

$$v = 0.18 - 0.49\left(\frac{\tau}{\tau_{\text{ult}}}\right) \geqslant 0.0094 \text{ N day/mm}. \quad (12c)$$

For $t_c = 7$ days

$$\alpha_1 = 10 \text{ mm/N}, \quad (13a)$$

$$\alpha_2 = 0.0008 \text{ mm/N}, \quad (13b)$$

$$v = 0.0094 \text{ N day/mm}. \quad (13c)$$

When the time-before-loading is between one and seven days, interpolation between Eqs. (12) and (13) can be used to predict the modeling parameters. For times-before-loading greater than seven days, Eq. (13) can be used because the shear strength of epoxy adhesive will be fully developed after seven days. It is noted that the effect of epoxy adhesive layer thickness is not considered in the modeling process due to lack of sufficient numbers of data points. Further research is needed to consider this parameter in modeling. However, it is worth noting that Eqs. (10), (11), (12) and (13) were developed for an average epoxy layer thickness of 0.21 mm which is typical for FRP strengthening of concrete structures.

To examine the ability of the proposed rheological models, the prediction error (PE) between experimentally observed deformations and predicted deformations using the rheological models was evaluated for the testing data set. The PE is defined as

$$\text{PE} = \sqrt{\frac{\sum_{i=1}^{N}(x_{\text{exp}} - x_{\text{pred}})^2}{N}} \quad (14)$$

where x_{exp} is the experimentally measured deformation, x_{pred} the deformation predicted by the rheological models and N the number of testing data sets. A low PE indicates a good ability of the model to predict creep of epoxy at the concrete–FRP interfaces. Table 6 shows PE values for Findley and MM models. In terms of PE values, both models showed good predictability. It should be noted that the testing group data were not used in the training process to identify models parameters.

Table 6
Prediction error for Findley and proposed MM model for testing data set

Model	Specimen	PE (mm)
Findley	S7-F	0.087
	S8-F	0.197
	S9-F	0.209
	Mean	0.164
MM	S7-F	0.092
	S8-F	0.112
	S9-F	0.133
	Mean	0.112

Fig. 10 shows the experimental results and the time–deformation relation predicted by the rheological models for specimens, S7-F and S9-F. These specimens were not used for developing the model. As shown in Fig. 10, the MM model can properly simulate both the instantaneous and creep shear deformation of epoxy adhesive at the concrete–FRP interfaces even though epoxy layer thickness was not considered in the prediction of Eqs. (12) and (13). It is also obvious that the Findley model overestimates the creep shear deformation of the epoxy adhesive at the concrete–FRP interfaces.

In the present study, as shown in Fig. 4, the applied load was removed at time t_r for several specimens. To investigate the creep behavior for both loading and unloading stages, the principles of linear superposition of strain [27,28] were considered. In this approach, the unloading status was considered by application of a sustained load similar in magnitude but in opposite direction ($-P$). Therefore, the total applied loading after unloading is zero. The total deformation in the unloading stage can be evaluated by the summation of the long-term deformation (Eq. (9)) and the unloading long-term deformation. Model parameters α_1 and α_2 for loading can

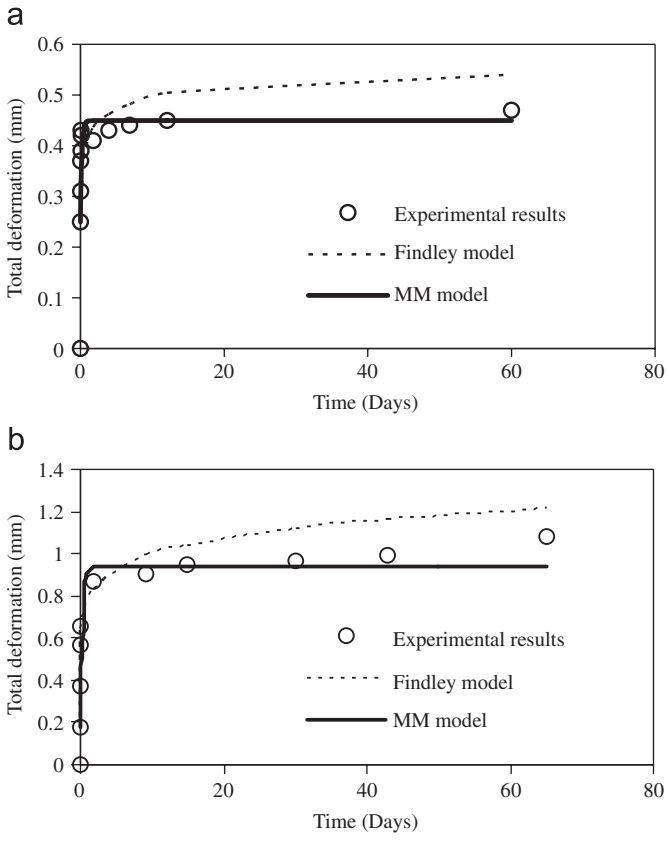

Fig. 10. Experimental and analytical results predicted by rheological models.

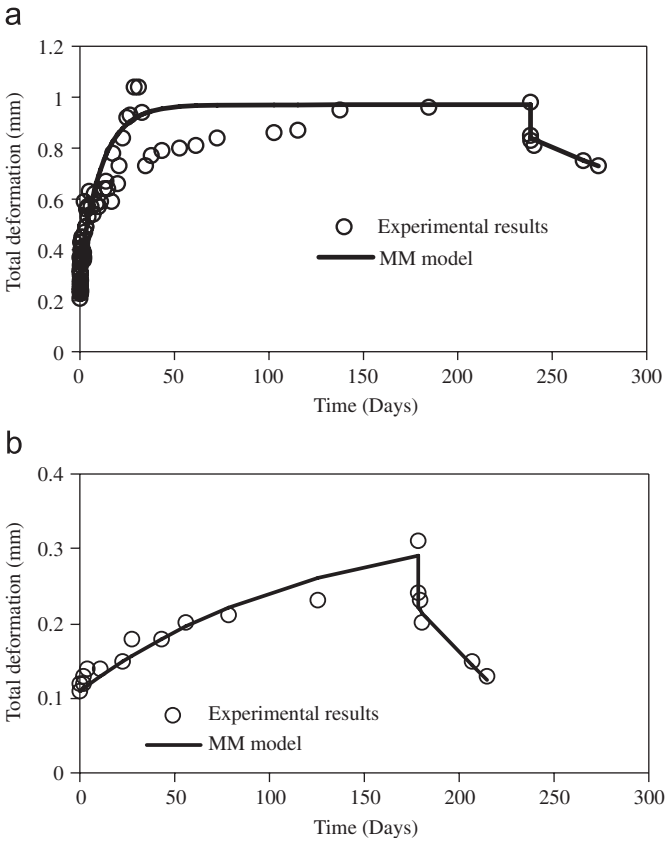

Fig. 11. Experimental and analytical results in loading and unloading stages.

be used for simulating the epoxy adhesive creep behavior under unloading while the time factor v for unloading shall be taken as $0.05t_r$ with t_r the time of unloading. Fig. 11 presents the creep behavior of epoxy for both loading and unloading stages. Fig. 11 shows that the MM model can simulate both loading and unloading creep observation for specimen, S1-B and S3-F with acceptable accuracy. It should be noted that a more complex rheological model with more springs and dashpots than the MM model may lead to better predictions of the rehological behavior of the concrete–FRP interface.

5. Conclusions

Shear creep experiments using double shear test set-up were performed to investigate the long-term behavior of epoxy adhesive at the concrete–FRP interfaces. Epoxy at the concrete–FRP interfaces was subjected to sustained shear stress for up to nine month time period. The experiments showed that epoxy at the concrete–FRP interfaces creeps, and that most of creep deformation develops within relatively short time period compared to the well known long creep time period of concrete. The experiments also showed that shear creep behavior of epoxy at concrete–FRP interfaces is dependent on the magnitude of shear stress to the ultimate shear strength and the time-before-loading. Furthermore, it was observed that high shear stress to ultimate shear strength can lead to unexpected failure at the concrete–FRP interfaces due to tertiary creep. This issue is not considered in current design guidelines for using FRP to strengthen RC structures. Further research is warranted to examine this concern.

Based on the experimental observations, creep of epoxy was modeled by means of two rheological models (Findley model and a new proposed MM model). Moreover, prediction equations for modeling parameters used in these models were developed, as function of applied shear stress to ultimate shear strength ratio and the time-before-loading. It is demonstrated that the proposed model can properly simulate the long-term creep behavior of epoxy adhesive at the concrete–FRP interfaces for both loading and unloading stages. The suggested rheological models are necessary for realistic finite element analysis of the interface zone under service loads. Such analysis is essential for realizing the effect of the viscoelastic behavior of the concrete–FRP interface components on FRP stress at cut off points, delamination propagation, concrete end cracking and possibility of creep rupture. Further research is underway to investigate the effect of other parameters such as the thermal conditions, the number of FRP layers and the use of mechanical anchors at the end of FRP sheets on the long-term behavior at the concrete–FRP interfaces.

Acknowledgments

Financial support by the University of New Mexico (UNM) and Defense Threat Reduction Agency (DTRA) is well appreciated. Special thanks for the technical staff at the Department of Civil Engineering UNM, especially Mr. Kenny Martinez for help to set-up creep experiments.

Appendix A. Evaluation of sustained shear stress

In double shear test, the sustained shear stress at front and back faces may be different even in a single specimen, due to the unexpected difference in shear stiffness in the epoxy material at both faces. In Fig. 6, the instantaneous shear deformations at front and back faces, $\Delta_{F16}(t_0)$ and $\Delta_{B16}(t_0)$, can be evaluated as

$$\Delta_{F16}(t_0) - \Delta_{16,FRP}(t_0) = 2\frac{\tau_F}{G_F}t_F, \tag{A.1a}$$

$$\Delta_{B16}(t_0) - \Delta_{16,FRP}(t_0) = 2\frac{\tau_B}{G_B}t_B, \tag{A.1b}$$

where τ_F and τ_B indicates the sustained shear stress at front and back faces, and G_F and G_B indicates the shear modulus at front and back faces. t_F and t_B indicates the epoxy thickness at front and back faces.

The summation of shear stress at front and back faces can be defined with the total applied load (P_T) applied to front and back faces.

$$\tau_F + \tau_B = \frac{P_T}{2A_0}, \tag{A.2}$$

where A_0 indicates bonded area of epoxy at a single concrete–FRP interface. Then, using $G_F = G_B$ and $t_F = t_B$, from Eqs. (A.1) and (A.2), the shear stress at each face can be defined as

$$\tau_F = \frac{P_T/(2A_0)}{1 + [\Delta_{B16}(t_0) - \Delta_{16,FRP}(t_0)]/[\Delta_{F16}(t_0) - \Delta_{16,FRP}(t_0)]}, \tag{A.3a}$$

$$\tau_B = \frac{P_T/(2A_0)}{1 + [\Delta_{F16}(t_0) - \Delta_{16,FRP}(t_0)]/[\Delta_{B16}(t_0) - \Delta_{16,FRP}(t_0)]}. \tag{A.3b}$$

Therefore, the sustained shear stress at each face can be determined by using the measured instantaneous shear deformation at each face.

References

[1] Emmons PH, Vaysburd AM, Thomas J. Strengthening concrete structure, part II. Concr Int 1998;20(4):56–60.
[2] Rizkalla S, Hassan T, Hassan N. Design recommendations for the use of FRP for reinforcement and strengthening of concrete structures. Prog Struct Eng Mater 2003;5(1):16–28.
[3] Roberts TM. Approximate analysis of shear and normal stress concentrations in the adhesive layer of plated RC beams. Struct Eng 1989;67(12):229–33.
[4] Ziraba YN, Baluch MH, Basunbul IA, Sharif AM, Azad AK, Al-Sulaimani AJ. Guidelines toward the design of reinforced concrete beams with external plates. Struct Eng 1994;91(6):639–46.
[5] Malek AM, Saadatmanesh H, Ehsani MR. Prediction of failure load of RC beams strengthened with FRP plate due to stress concentration at the pate end. Struct Eng 1998;95(2):142–52.
[6] Ahmed O, Gemert DV, Vandeewall L. Improved model for plate-end shear of CFRP strengthened RC beams. Cem Concr Compos 2001; 23(1):3–19.
[7] Coronado CA, Lopez MM. Modeling of FRP–concrete bond using nonlinear damage mechanics. In: Proceedings of the seventh international symposium on fiber reinforced polymer (FRP) reinforcement for concrete structures, Kansas City, MO, SP-230-22; November 6–9, 2005.
[8] Teng JG, Chen JF, Smith ST, Lam L. FRP strengthened RC structures. Wiley: England; 2002.
[9] Hiroyuki Y, Wu Z. Analysis of debonding fracture properties of CFS strengthened member subject to tension. In: Proceedings of third international symposium on non-metallic (FRP) reinforcement for concrete structures, Sapporo, Japan; 1997. p. 287–94.
[10] Savoia BF, Mazzoth C. A numerical model for FRP–concrete delamination. Compos Part B Eng 2006;37(4–5):356–64.
[11] Pecce M, Ceroni F. Modeling of tension-stiffening behavior of reinforced concrete ties strength with fiber reinforced plastic sheets. ASCE J Compos Constr 2004;8(6):510–8.
[12] Tounsi A, Benyoucef S. Interfacial stresses in externally FRP-plated concrete beams. Int J Adhes Adhes 2007;27(3):207–15.
[13] Shrive NG, Reda Taha MM. Effect of creep on new masonry structures. In: Binda L, editor. Learning from failure, long-term behavior of heavy masonry structures. South Hampton, UK: WIT Press; 2007. p. 83–105 [Chapter 4].
[14] Yang QS, Peng XR, Kwan AKH. Finite element analysis of interfacial stresses in FRP–RC hybrid beams. Mech Res Commun 2004;31(3):331–40.
[15] ASTM C 39/C 39M-04a. Standard test method for compressive strength of cylindrical concrete specimens. West Conshohocken, PA: ASTM; 2005. p. 7.
[16] Findley WN, Lai JS, Onaran K. Creep and relaxation of nonlinear viscoelastic material. NY, USA: Dover Publication; 1989.
[17] Shrive NG, Sayed-Ahmed EY, Tilleman D. Creep analysis of clay masonry assemblages. Can J Civil Eng 1997;24(3):367–79.
[18] ACI Committee 440. Guide for the design and construction of externally bonded FRP systems for strengthening concrete structures (ACI 440.2R-02). Michigan: American Concrete Institute; 2002.
[19] Shrive NG, Reda Taha MM, Masia MJ. Restoration and strengthening with fiber reinforced polymers. Struct Anal Hist Constr 2005;1:829–35.
[20] Zou PXW. Long-term properties and transfer length of fiber-reinforced polymers. J Compos Constr 2003;7(1):10–9.
[21] Neville AM, Dilger WH, Brooks JJ. Creep of plain and structural concrete. New York, USA: Longman Inc.; 1983.
[22] Hansen TC. Theories of multi-phase materials applied to concrete, cement mortar and cement paste. In: Proceedings of the international conference on the structure of concrete. London: Cement and Concrete Association; 1968. p. 24–36.
[23] Lenczner D. Creep and prestress losses in brick masonry. Struct Eng 1986;64B(3):57–62.
[24] Rangaraj SV, Smith LV. The nonlinear viscoelastic response of a wood–thermoplastic composites. Mech Time Dependent Mater 1999; 3:125–39.
[25] Findley WN. Mechanism and mechanics of creep of plastics. SPE J Soc Plast Eng 1960;16(1):57–65.
[26] Zienkiewicz OC, Cormeau IC. Viscoplasticity–plasticity and creep in elastic solids. Int J Numer Methods Eng 1974;8:821–45.
[27] Findley WN, Khosla G. Application of the superposition principle and theories of mechanical equation of state, strain and time hardening to creep of plastics under changing loads. Appl Phys Lett 1995;26(7):821–32.
[28] Hibbler RC. Mechanics of materials. 6th ed. Uppersaddle River, NY, USA: Pearson, Prentice-Hall; 2005.